processes

MDPI

Article

Research on the Pressure Relief Mechanism of Gently Inclined Long-Distance Lower Protective Layer Mining and Cooperative Gas Control Technology

Yanjun Tong [1], Qian Liu [2,*], Qinming Wang [1], Chuanjie Zhu [3,*] and Yue'e Wu [3]

[1] Coal Mining and Utilization Research Institute, Pingdingshan Tianan Coal Mining Co., Ltd., Pingdingshan 467000, China
[2] School of Resource Engineering, Longyan University, Longyan 364012, China
[3] School of Safety Engineering, China University of Mining and Technology, Xuzhou 221116, China
* Correspondence: liuqian_919@163.com (Q.L.); anq021@126.com (C.Z.); Tel.: +86-15280812578 (Q.L.); +86-15950674572 (C.Z.)

Abstract: This study investigates pressure relief mechanisms and gas migration control in gently inclined remote lower protective layer mining, using the $Wu_{8\text{-}31220}$ working face of Pingdingshan Tianan Coal Industry's No. 1 Mine as a prototype. The integrated approach combining theoretical modeling with multidimensional monitoring systems yielded critical insights into pressure relief patterns. Analysis demonstrated dip-oriented pressure relief angles measuring 77° (intake side) and 83° (return side), collectively establishing a pressure relief zone spanning 160.5 m. Concurrently, horizontal pressure relief angles were determined to be 60° in both orientations, generating a pressure relief zone extending 1261 m. Mechanical monitoring revealed multistage "compression–expansion" responses in the Ding6 seam during protective seam extraction, achieving maximum expansion deformations of 9.89–13.55‰ within the boundary zone. By optimizing borehole spacing (20 m) and extraction duration (8 months), the $Ding_{6\text{-}32070}$ working face extracted 1.18 million m^3 of gas (31.22% reserves), resolving spatial coupling challenges between gas recovery efficiency and pressure relief dimensions. This work advances understanding of pressure relief and permeability enhancement in gently inclined remote lower protective layer mining. The findings provide both theoretical foundations and technical benchmarks for safe deep coal mining operations and efficient gas control strategies.

Keywords: lower protective seam; protective range; gas pressure; expansion deformation; pressure relief gas

check for updates

Academic Editor: Fabrizio Scala

Received: 19 April 2025
Revised: 22 May 2025
Accepted: 23 May 2025
Published: 25 May 2025

Citation: Tong, Y.; Liu, Q.; Wang, Q.; Zhu, C.; Wu, Y. Research on the Pressure Relief Mechanism of Gently Inclined Long-Distance Lower Protective Layer Mining and Cooperative Gas Control Technology. *Processes* **2025**, *13*, 1656. https://doi.org/10.3390/pr13061656

Copyright: © 2025 by the authors. Licensee MDPI, Basel, Switzerland. This article is an open access article distributed under the terms and conditions of the Creative Commons Attribution (CC BY) license (https://creativecommons.org/licenses/by/4.0/).

1. Introduction

Energy is the cornerstone and key element of national economic and social sustainable development [1], and coal is the ballast stone for ensuring China's energy security, holding an irreplaceable position [2–4]. However, with the depletion of shallow coal resources, coal mines have entered the era of deep coal resource mining, facing increasingly complex scientific and technical problems [5–7], especially coal and gas outbursts, which have become a major challenge for coal mine safety production [8–11]. China confronts the most severe challenges in coal and gas outburst control worldwide [12,13]. These dynamic failures have triggered multiple catastrophic mining accidents, resulting in significant casualties and substantial economic losses [14]. Industry statistics reveal that Chinese coal mines persistently lead global rankings in both outburst incident frequency and casualty rates [15].

To address this critical safety challenge, researchers and engineering experts have developed a comprehensive prevention and control technology system through sustained research efforts. This system integrates multidimensional approaches, including regional prediction, advanced detection, and pressure relief drainage technologies [16–19]. Among the countermeasures, protective layer mining is one of the most effective regional measures [20–22]. In the gas outburst mine, the coal seam with less than zero outburst danger is first mined, as it can eliminate or weaken the outburst danger of adjacent coal seams and is therefore referred to as a protective layer [23]. Protective layer mining has two types based on stratigraphic positioning relative to outburst-prone coal seams: lower protective layer mining (protective layer beneath protected layer) and upper protective layer mining (protective layer above protected layer) [24]. There exists a fundamental distinction between single-seam mining and protective layer mining in terms of technical principles and engineering implementation [25]. During protective layer mining, systematic gas drainage engineering must be concurrently implemented to effectively control gas emissions in the pressure-relieved zones [26]. If protective layer mining is conducted without accompanying control measures, it will not only fail to achieve effective gas management in outburst coal seams but may also induce major gas accidents due to mining-induced stress disturbances [27]. Therefore, accurately delineating pressure relief zones following protective seam extraction and optimizing associated technical control measures constitutes a critical engineering imperative for enhancing coal mine safety.

Building on this foundation, researchers have undertaken empirical investigations to elucidate the mechanistic relationships between protective layer mining practices and gas control efficacy. Liu et al. [28] demonstrated through integrated physical simulation experiments and FLAC3D numerical modeling that upper protective seam extraction results in 86.2% pressure relief in underlying coal strata, with associated strike-oriented dilatational strain attaining a maximum value of 11.3‰. Cheng et al. [29] investigated the spatial permeability distribution within a protected coal seam during protective coal seam mining and strategically optimized gas drainage borehole layouts to align with the identified permeability zonation. Li et al. [30] investigated fracture network evolution and pressure relief mechanisms in the protected coal seam post-protective layer mining, revealing a 50.7% gas pressure reduction and 68.67% residual gas content decline relative to original seam conditions. Xie et al. [25] combined theoretical analysis, numerical simulation, and field tests to investigate how fracture evolution and permeability changes were induced by upper protective coal seam mining, finding that the maximum expansion deformations occurred near the open cut and the mining end line of the working face. Zhang et al. [24] used FLAC3D to analyze the stress evolution and deformation laws of the overlying coal seam, finding that the stress distribution in the strike direction can be divided into the original stress zone, pressure relief zone, and stress concentration zone. Jin et al. [31] analyzed the impact of remote lower protective layer mining on coal mine gas control, finding that the maximum expansion deformation rate of the protected seam reached 33.4‰ after protective layer mining, and the permeability of the coal seam increased significantly by 4320 times. Wang et al. [32] selected a soft rock layer as the protective seam in the Luling Coal Mine in Huaibei, and through numerical simulation, found that the soft rock layer was within the effective protection range of the 8–9 and 10 coal seams, and the expansion deformation of the protected seam reached 4.1‰ after mining. Lu et al. [23] revealed through PFC simulations that rock arch structures mechanically redirect overburden loads toward the goaf periphery, while fractured strata act as stress barriers, inhibiting stress propagation; larger mining dimensions intensify pressure relief effects, whereas greater interlayer spacing or enhanced rock strength diminish these effects.

The existing research on protective seam mechanisms has established a theoretical framework through systematic investigations into stress redistribution, strata deformation patterns, permeability evolution, and gas migration dynamics, providing essential guidance for conventional mining operations. Nevertheless, these achievements remain constrained by oversimplified geological models, particularly in addressing the engineering challenges of deep multi-seam extraction characterized by substantial interlayer distances and intricate stress–permeability coupling mechanisms.

The Pingdingshan mining area, a strategic coal production base in central China, presents representative deep-mining geological conditions with Carboniferous–Permian coal measures extending to 800 m depths. This distinctive geological profile, characterized by thrust nappe tectonics (a structural feature formed through compression-induced overlapping of rock strata) [33] and significant geostatic stress accumulation, establishes an essential cognitive framework for geomechanical studies in deep-mining engineering. The region's Ding-Wu-Ji coal seam groups exhibit the following distinctive characteristics: macro-scale interlayer spacing contrasting with micro-scale intralayer compactness, compounded by ultralow permeability, hyperbaric gas reservoirs, and structural complexity [34]. Of particular significance is the Pingmei No. 1 Mine, an exemplar site for multi-seam cluster extraction. This investigation conducts a specialized examination of long-distance protective layer mining operations (defined as interlayer spacing exceeding 60 m between protective and protected strata) in deep extraction engineering by (1) quantitatively assessing the multistage transmission effects of protective layer techniques on key safety indicators; (2) systematically evaluating its gas migration control mechanisms under ultra-deep mining configurations. The findings establish vital engineering precedents for safe resource recovery in analogous geoenvironments.

2. Project Overview

2.1. Mine Overview

Pingdingshan Tianan Coal Industry Co., Ltd. No. 1 Mine is located in the middle of the Pingdingshan mine field, covering an area of about 29.3 km^2, mainly mining the Ding and Wu coal resources. The Ding group mainly mines the $Ding_5$ and $Ding_6$ coal seams, while the Wu group mainly mines the Wu_8, W_9, and W_{10} coal seams. The $Ding_6$ coal seam is an outburst coal seam, with an average distance of 75 m from the Wu_8 coal seam.

2.2. Working Face Overview

(1) Protective Seam

The $Wu_{8\text{-}31220}$ working face is located in the western section of the $Wu_{\text{-}1}$ dip mining district at the Third Level. The elevation of the working face ranges from −729 m to −839 m, corresponding to a burial depth between 870 m and 1039 m. The working face is 1340 m long and 177 m wide, with an average mining height of 2.0 m. The coal seam dip angle is 12~16°, with an average of 14°. The immediate roof is mudstone, 4.5~7.5 m thick; the main roof is quartz sandstone, 4.5~14.5 m thick. The immediate floor is mudstone, 10.7~15.4 m thick; the main floor is medium-grained sandstone, 10.5~18.5 m thick.

(2) Protected Seam

The $Ding_{6\text{-}32070}$ working face is located in the east wing of the third level Ding-2 mining area, with an elevation of −643 to −718 m. The working face is 1210 m long and 200 m wide, with an average mining height of 2.2 m. The predicted gas content of the $Ding_{6\text{-}32070}$ working face is 5.27 m^3/t, and the predicted gas pressure is 0.58 MPa, making it an outburst working face.

3. Theoretical Analysis of the Protective Range of Protective Layer Mining

3.1. Along the Dip Direction

Protective layer mining induces progressive strata movement and structural reorganization, activating stress-redistribution mechanisms within overlying protected seams [35–37]. The mechanistic comprehension of these stress redistribution patterns carries critical engineering significance. Deficient understanding frequently manifests as suboptimal gas drainage performance in protected zones, culminating in missed extraction windows and persistent outburst hazards. This geomechanical process generates the following dual synergistic effects: (1) fracture-driven permeability enhancement via interconnected fracture network development, and (2) gas desorption–diffusion acceleration due to pressure gradient shifts. These synergistic processes dynamically define the stress relief protective zone, whose spatiotemporal boundaries are governed by the pressure relief angle (θ)—a geotechnical parameter critically dependent on the seam dip angle (α). As empirically codified in China's technical specifications for coal and gas outburst prevention, θ-α correlations exhibit nonlinear behavior across dip angle regimes (see Table 1).

Geomechanical analysis shows that the $Wu_{8\text{-}31220}$ working face has an average dip angle of 14°. Following the engineering geological parameter rounding principle, the pressure relief angles are determined as $\delta_1 = 77°$ (intake side) and $\delta_2 = 83°$ (return side). Consequently, in the dip-oriented configuration, the lower protective boundary of the $Ding_{6\text{-}32070}$ working face is strategically offset inward by 17.3 m relative to the $Wu_{8\text{-}31220}$ intake roadway, while the upper protective boundary exhibits a measured 9.2 m inward displacement from the $Wu_{8\text{-}31220}$ return roadway. Under the engineering disturbance caused by mining the Wu_8 coal seam, the theoretical pressure relief protection range extending along the stratigraphic dip direction of the $Ding_6$ coal seam spans 160.5 m, as systematically detailed in Figure 1.

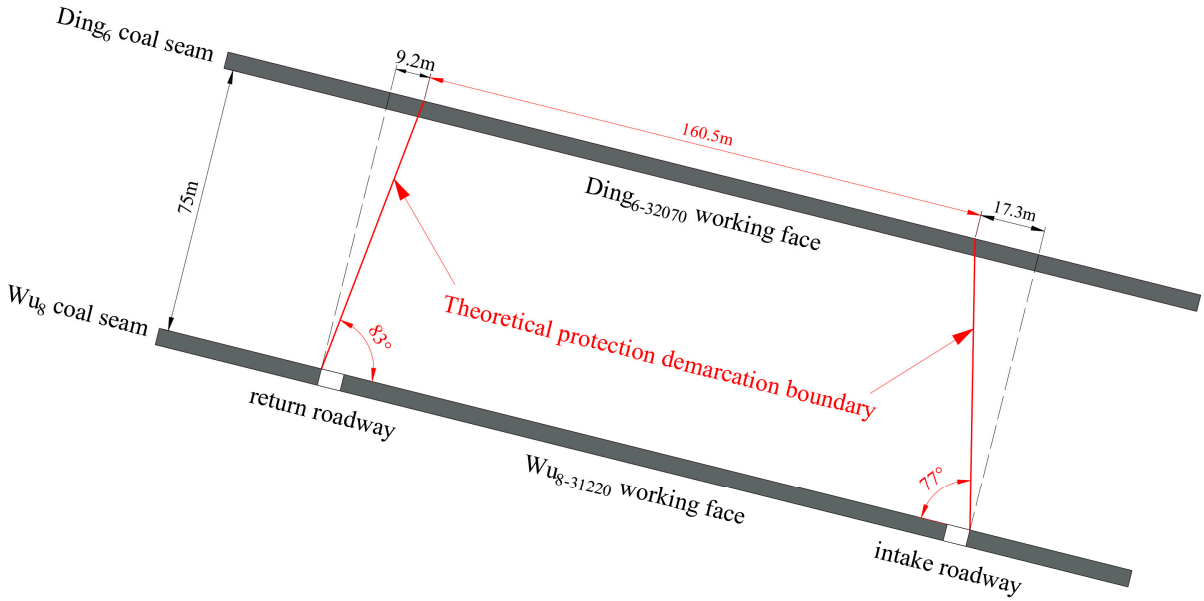

Figure 1. Schematic diagram of the influence range of the $Ding_{6\text{-}32070}$ working face in dip direction after mining of the $Wu_{8\text{-}31220}$ working face.

Table 1. Pressure relief angle of the protective layer along the inclined direction.

Coal Seam Dip Angle α/°	Pressure Relief Angle δ/°			
	δ_1	δ_2	δ_3	δ_4
0	80	80	75	75
10	77	83	75	75
20	73	87	75	75
30	69	90	77	70
40	65	90	80	70
50	70	90	80	70
60	72	90	80	70
70	72	90	80	72
80	73	90	78	75
90	75	90	75	80

3.2. Along the Strike Direction

A strategically implemented 3-month interval between the cessation of the $Wu_{8\text{-}31220}$ working face and the initiation of $Ding_{6\text{-}32070}$ face mining creates an optimized pressure-relief temporal window. This temporal coordination ensures sufficient pressure relief in $Ding_6$ seam. The strike pressure relief angle of the Wu_8 working face is thus determined as 60° through comprehensive evaluation. Theoretical investigations demonstrate a precisely maintained 43 m inward offset between the $Ding_{6\text{-}32070}$ protection zone and both the initiation/termination boundaries of the Wu_8 working face, as shown in Figure 2.

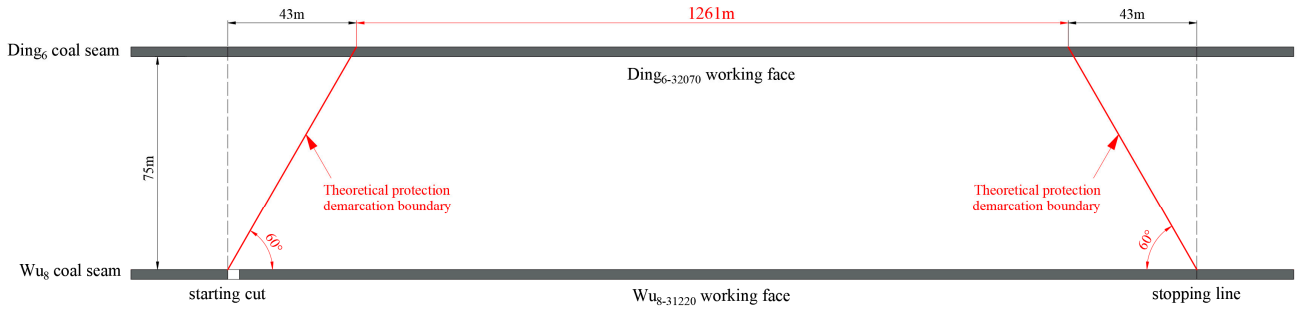

Figure 2. Schematic diagram of the influence range of the $Ding_{6\text{-}32070}$ working face in strike direction after mining of the $Wu_{8\text{-}31220}$ working face.

4. Field Parameter Testing Layout Plan

4.1. Gas Pressure Testing in the $Ding_6$ Coal Seam

4.1.1. Borehole Layout

To quantitatively characterize the pressure relief domains along both ventilation flanks of the $Ding_6$ coal seam following Wu_8 seam extraction, a systematic monitoring protocol was implemented. Three diagnostic boreholes were strategically positioned in the high-level drainage roadway of the $Wu_{8\text{-}31220}$ and $Wu_{8\text{-}31200}$ intake roadway, respectively. These boreholes were aligned perpendicular to the demarcation boundary of the $Ding_{6\text{-}32070}$ protective coverage zone with 15 m bilateral extensions, establishing a comprehensive pressure monitoring matrix. The geometrically optimized borehole array configuration is explicitly detailed in Figure 3.

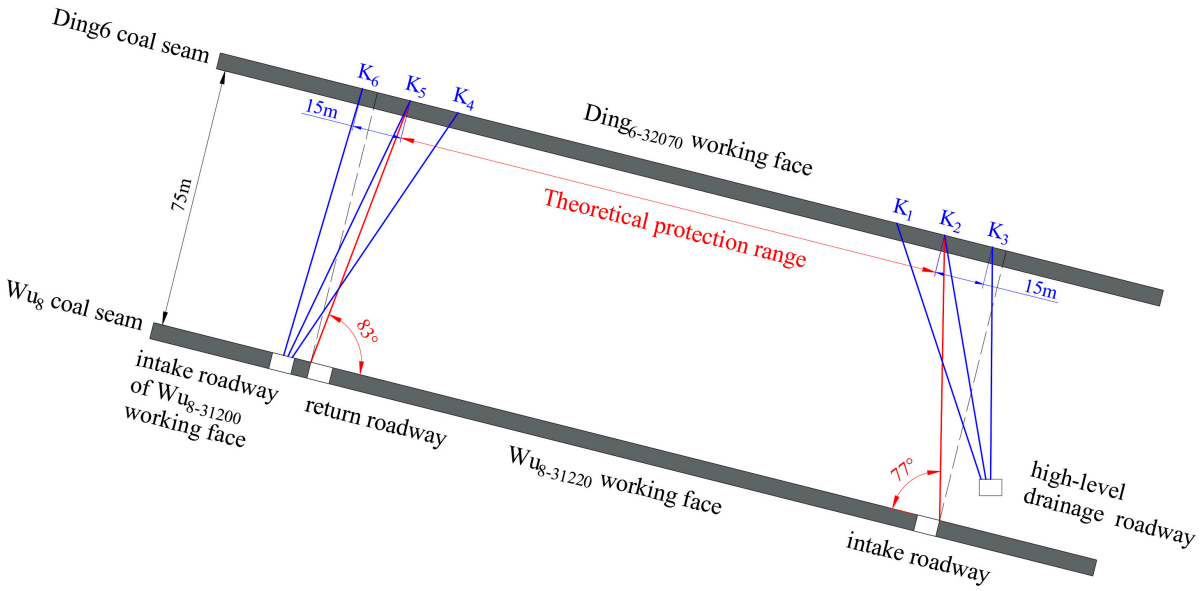

Figure 3. Profile map of borehole layout for dip unloading investigation of $Ding_{6\text{-}32070}$ working face.

To quantitatively delineate the pressure relief domains along both initiation and termination boundaries of the $Ding_6$ coal seam post-Wu_8 seam extraction, a diagnostic borehole array was strategically implemented. Three pressure-monitoring boreholes were precisely configured at each extremity of the gas drainage roadway in the $Wu_{8\text{-}31220}$ intake roadway, orthogonally aligned with the $Ding_{6\text{-}32070}$ protective coverage demarcation boundary with 15 m symmetric offsets. This geometrically constrained monitoring network established a pressure evolution matrix, with the optimized borehole array geometry systematically illustrated in Figure 4. The design parameters of gas pressure test boreholes for $Ding_{6\text{-}32070}$ working face are summarized in Table 2.

Table 2. Design parameters for gas pressure test boreholes for $Ding_{6\text{-}32070}$ working face.

Borehole No.	Borehole Collar Location		Terminal Borehole Position	Azimuth Angle/°	Dip Angle/°	Borehole Diameter/mm	Sealing Depth/m	Borehole Length/m
K_1	$Wu_{8\text{-}31220}$ high-level drainage roadway	400 m from the opening	15 m inside the demarcation boundary	191	55	94	85	90
K_2			On the demarcation boundary	191	65	94	80	84
K_3			15 m outside the demarcation boundary	191	70	94	80	85
K_4	$Wu_{8\text{-}31200}$ intake roadway	610 m from the opening	15 m inside the demarcation boundary	11	59	94	78	82
K_5		600 m from the opening	On the demarcation boundary	11	69	94	72	77
K_6		590 m from the opening	15 m outside the demarcation boundary	11	81	94	72	76
K_7	$Wu_{8\text{-}31220}$ high-level drainage roadway	65 m from the starting cut	15 m inside the demarcation boundary	191	60	94	85	90
K_8		50 m from the starting cut	On the demarcation boundary	191	55	94	80	85
K_9		35 m from the starting cut	15 m outside the demarcation boundary	191	55	94	82	86
K_{10}	$Wu_{8\text{-}31220}$ high-level drainage roadway	127 m from the return airway	15 m inside the demarcation boundary	191	57	94	79	82
K_{11}		112 m from the return airway	On the demarcation boundary	191	55	94	82	86
K_{12}		97 m from the return airway	15 m outside the demarcation boundary	191	60	94	80	85

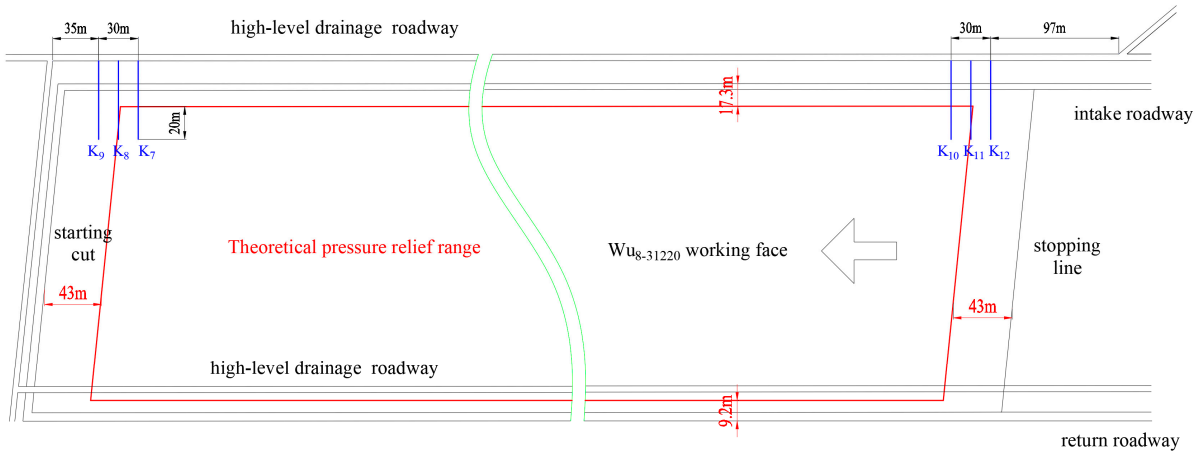

Figure 4. Plan view of borehole layout for strike unloading investigation of $Ding_{6\text{-}32070}$ working face.

4.1.2. Sealing Method

The gas pressure testing in the $Ding_6$ coal seam adopted the inflatable bag/cement slurry pressure grouting sealing method. The schematic diagram illustrating the gas pressure testing methodology for the $Ding_{6\text{-}32070}$ working face is depicted in Figure 5. The pressure measurement system was constructed using a 15 mm diameter aluminum–plastic composite tube, incorporating a filter screen assembly at its leading end. Two inflatable bags were securely mounted at predetermined positions along the tube's leading section, maintaining an 8 m interval between the first and second bags. Following the specified sealing depth requirements, the assembled tubing system was carefully deployed into the borehole. Upon successful positioning of the bags, grouting operations were initiated and continued until achieving stable grout consolidation. Subsequently, the pressure gauge was calibrated and installed, followed by the commencement of continuous gas pressure monitoring. The deployed pressure measurement device constituted a YB-150A/B series gauge produced by Shanghai Yichuan Instrument Factory, featuring a 0–1 MPa measurement range with 0.4-grade precision (maximum permissible error: ±0.004 MPa).

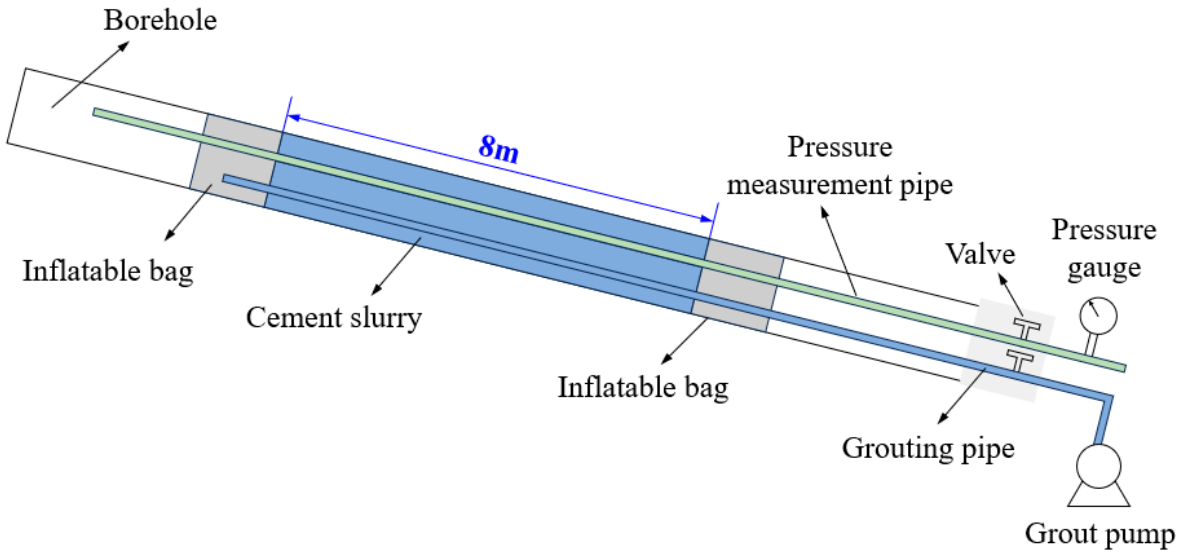

Figure 5. Schematic diagram of the pressure grouting seal method using bag/cement slurry for $Ding_{6\text{-}32070}$ working face.

4.2. Expansion Deformation Testing in the Ding$_6$ Coal Seam

Following protective seam extraction, significant pressure relief and structural expansion develop within the overlying protected seam [25,31]. This expansion deformation serves as a critical parameter for assessing the efficacy of protective layer mining operations. A monitoring network comprising six boreholes (designated P1–P6) was strategically deployed along the Wu$_{8\text{-}31220}$ intake airway's high-level drainage roadway to quantify coal mass deformation in the Ding$_{6\text{-}32070}$ working face. The borehole array spanned strategic positions at 350 m (P1), 550 m (P2), 800 m (P3), 1000 m (P4), 1100 m (P5), and 1200 m (P6) from the longwall starting cut, with terminal points aligned along the intake airway's demarcation boundary.

The expansion deformation monitoring system employed the high-precision LBY-3A stratigraphic displacement monitor, which features a maximum range of 200 mm and a display resolution of 1 mm. This dual-anchor instrumentation comprises the following: (1) a roof anchor head securely embedded within the Ding6 coal seam's upper lithological boundary, and (2) a corresponding floor anchor head embedded within the seam's basal stratum. Through the real-time tracking of differential displacement between these geomechanical reference points, the system enables the continuous quantification of coal seam deformation parameters. A schematic representation of this monitoring methodology's operational framework is presented in Figure 6.

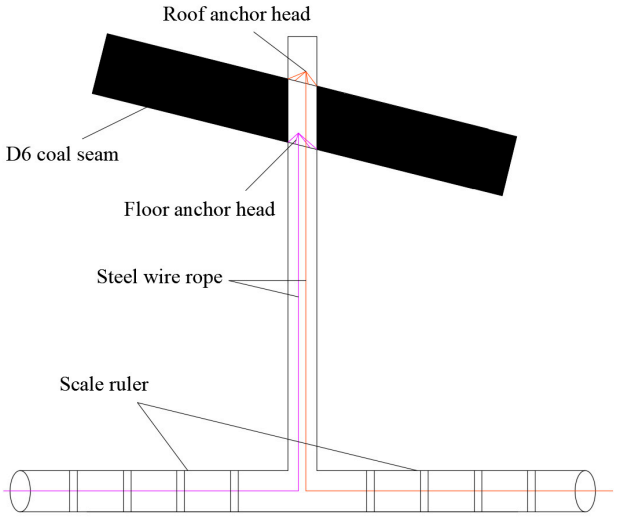

Figure 6. Schematic diagram of monitoring the expansion deformation of Ding$_{6\text{-}32070}$ working face.

4.3. Design of Pressure Relief Gas Extraction Boreholes in the Ding$_6$ Coal Seam

Pressure Relief Gas Drainage System Design for Ding$_6$ Coal Seam

The borehole array was strategically designed in the Wu$_{8\text{-}31220}$ intake airway's high-level drainage roadway, comprising 58 cross-strata boreholes penetrating into the Ding$_6$ protected seam. The layout diagram of gas extraction boreholes for the depressurized Ding$_{6\text{-}32070}$ working face is depicted in Figure 7. All borehole endpoints are positioned 15 m inside the boundary line of the Ding$_6$ coal seam's intake roadway side, with a spacing of 20 m between boreholes. The boreholes have a depth of 72.25 m and a dip angle of 51°. The 1#–40# boreholes are designated as the first extraction unit, while the 41#–58# boreholes form the second extraction unit. The first extraction unit commenced networked extraction on 23 October 2023, whereas the second extraction unit initiated networked extraction earlier on September 5 of the same year. This extraction operation aims to fully utilize the influence of Wu$_8$ coal seam mining on the Ding$_6$ coal seam, achieving pressure relief gas extraction from the distant protected Ding$_6$ coal seam layer.

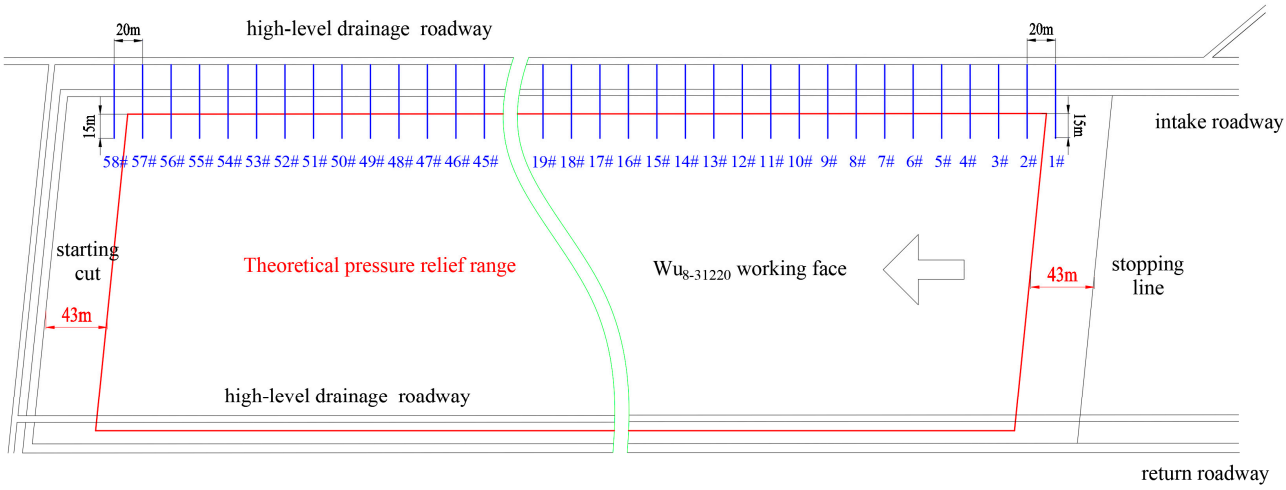

Figure 7. Layout diagram of gas extraction boreholes for the depressurized $Ding_{6\text{-}32070}$ working face.

5. Analysis of the Effect of Remote Protective Layer Mining

5.1. Gas Pressure in the $Ding_6$ Coal Seam

The gas pressure test results of the $Ding_{6\text{-}32070}$ working face are shown in Figure 8. Along the dip direction, intake airway measurements demonstrate a progressive pressure reduction from 0.62 MPa at 15 m extra-boundary positions to 0.20 MPa at boundary interface and 0.18 MPa intra-boundary, while return airway counterparts record 0.61 MPa (extra-boundary), 0.28 MPa (boundary), and 0.31 MPa (intra-boundary). Strike direction measurements show similar patterns, e.g., the starting cut areas exhibit 0.63 MPa extra-boundary pressure decreasing to 0.18 MPa at boundary and 0.15 MPa internally, whereas stopping line zones maintain 0.63 MPa extra-boundary with sequential reductions to 0.36 MPa (boundary) and 0.24 MPa (intra-boundary). These measurements confirm the defined boundary's effectiveness as a pressure discontinuity, with extra-boundary pressures maintaining near-original reservoir levels (0.61–0.63 MPa) versus significantly reduced intra-boundary values (0.15–0.36 MPa), demonstrating differential pressure relief responses across directional orientations.

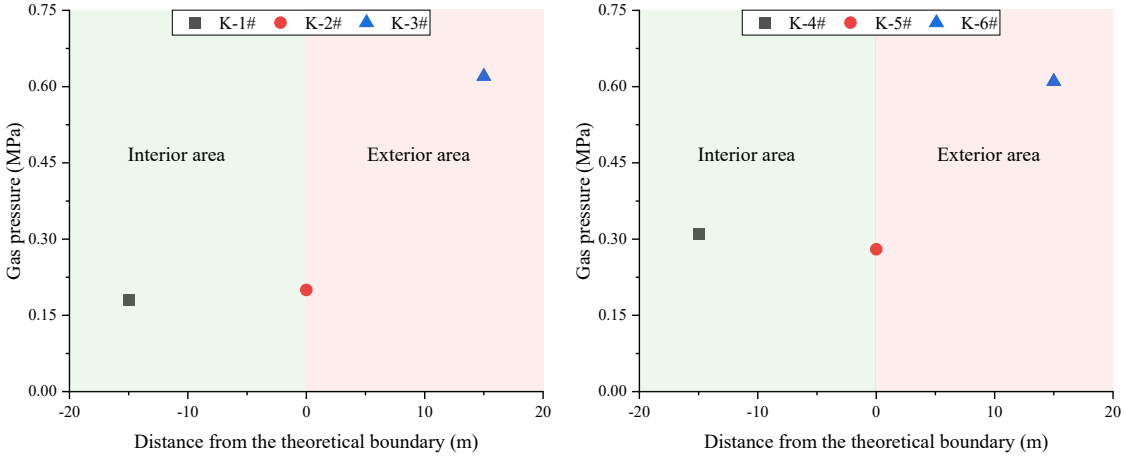

(**a**) Dip direction of the intake roadway side (**b**) Dip direction of the return roadway side

Figure 8. *Cont.*

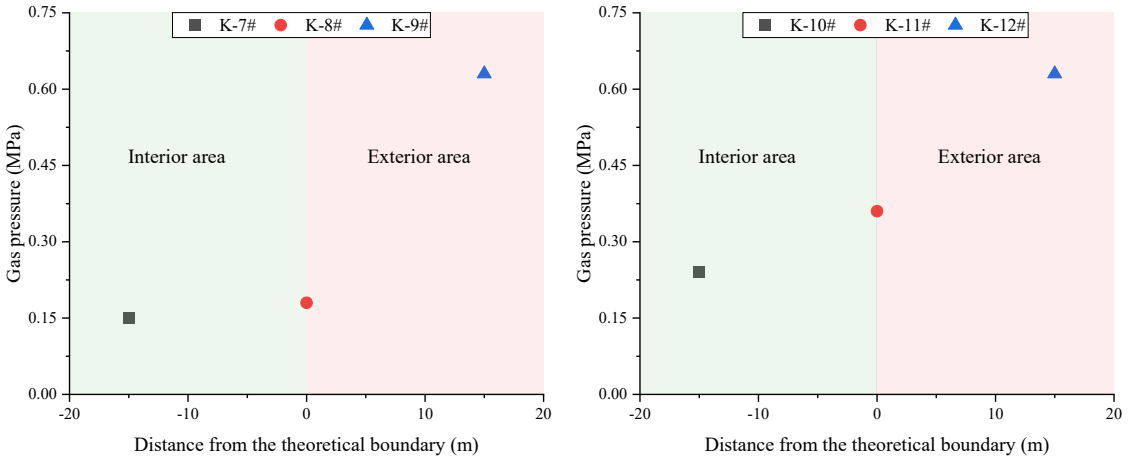

(**c**) Strike direction of the starting cut side (**d**) Strike direction of the stopping line side

Figure 8. Results of gas pressure measurement in $Ding_{6\text{-}32070}$ working face.

Gas pressure measurements demonstrate the following distinct zonal characteristics across spatial domains: within 15 m inside the defined boundary, pressures register 0.15~0.31 MPa; at the boundary interface, 0.18–0.36 MPa; and at 15 m beyond the boundary, 0.61–0.63 MPa. These measurements reveal that extra-boundary pressures approximate original reservoir conditions (0.61~0.63 MPa), indicating negligible mining-induced disturbance from the $Wu_{8\text{-}31220}$ working face in peripheral zones. Conversely, both boundary-proximal and intra-boundary regions exhibit significantly reduced pressures (32–52% of original levels), demonstrating effective pressure relief effects from extraction activities within the defined boundary. This pressure gradient establishes the demarcation boundary as the critical transition zone between disturbed and undisturbed reservoir states, thereby serving as the operational threshold for gas pressure relief demarcation in mining-impacted strata.

5.2. Expansion Deformation of the $Ding_6$ Coal Seam

Test points P_1, P_2, P_3, P_4, P_5, and P_6 recorded the expansion deformation of the $Ding_6$ coal seam within a range of 80 m in front and 200 m behind. The expansion deformation of the $Ding_6$ coal seam changes with the advance of the $Wu_{8\text{-}31220}$ working face, as shown in Figure 9. In the figure, negative values on the horizontal axis indicate that the advancing working face has not yet reached the test position; negative values on the vertical axis indicate that the $Ding_6$ coal seam is in a compressed state.

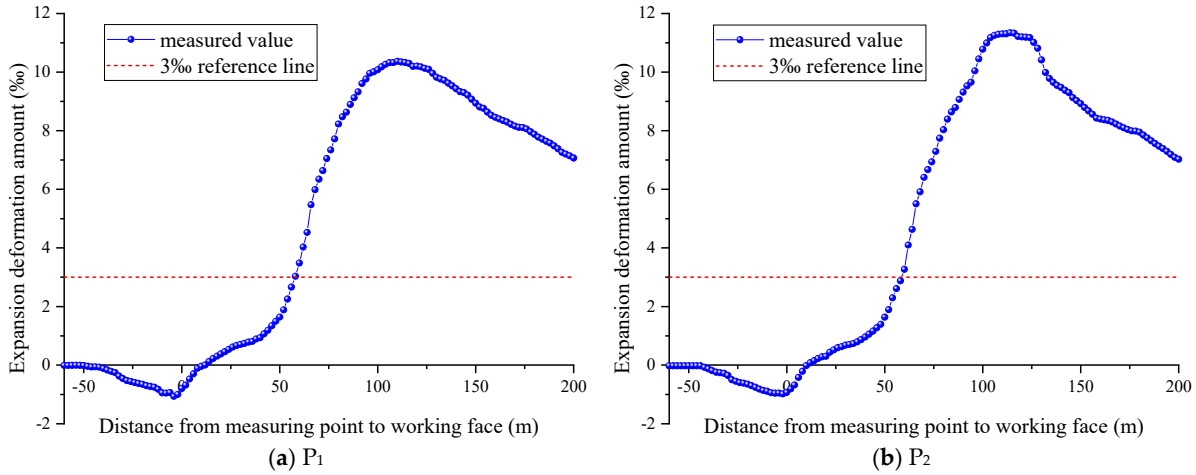

(**a**) P_1 (**b**) P_2

Figure 9. *Cont.*

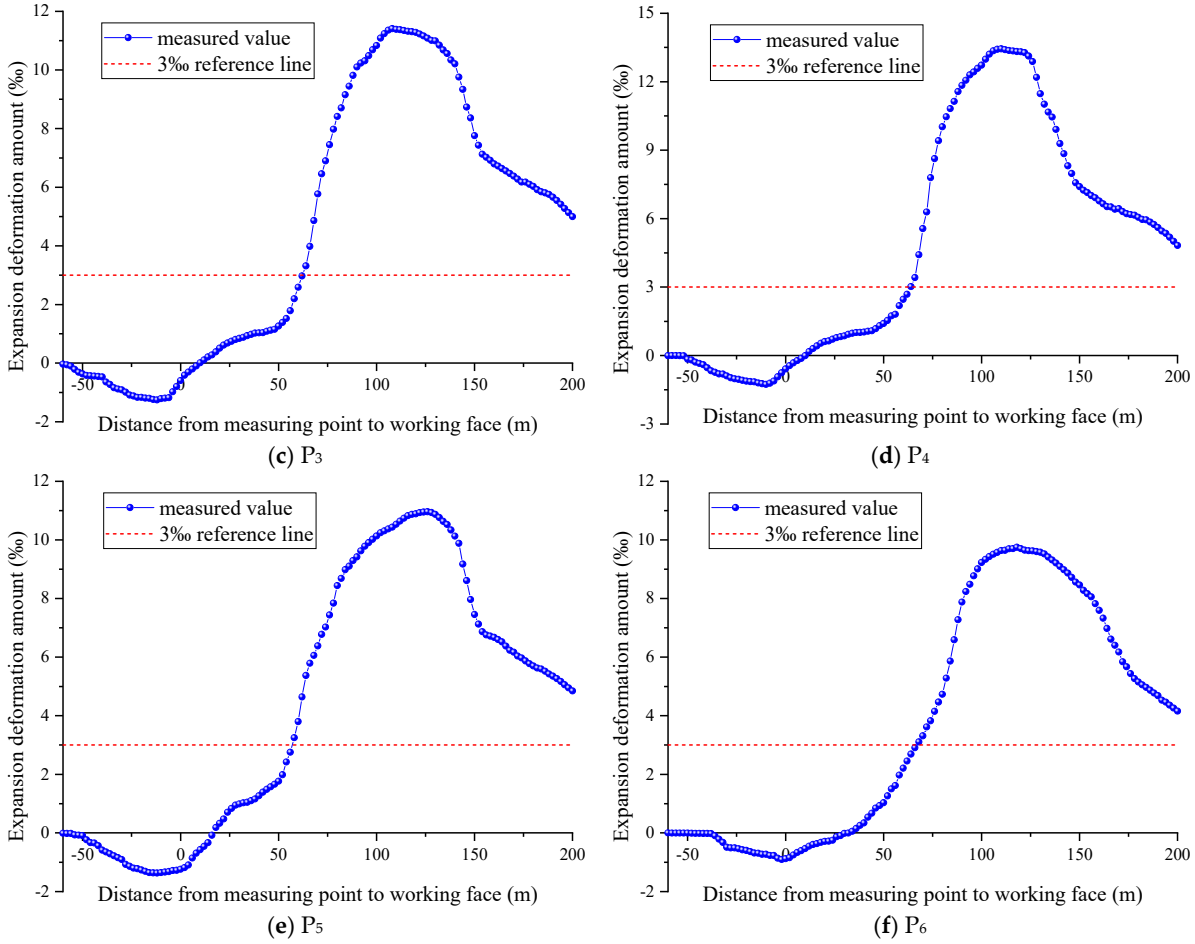

Figure 9. Observation results of expansion deformation in $Ding_{6\text{-}32070}$ working face.

From the figure, it can be observed that during the advance of the working face, the $Ding_6$ coal seam undergoes a process of first compression and then expansion, which is related to the distribution of support pressure along the strike direction of the working face [38,39]. As the working face approaches the test point, the coal seam begins to be compressed at a distance of 50 m (−50 m) from the test point. Subsequently, as the distance to the test point gradually decreases, the coal seam continues to be further compressed until it reaches the maximum compression at a distance of 3~0 m (−3~0 m) from the test point. However, as the working face moves away from the test point, the coal seam begins to transition from a compressed state to an expanded state, with the critical point of compression and expansion at a distance of 10 m from the test point. After that, the expansion deformation increases rapidly, reaching the maximum value at a distance of about 115 m from the test point. After 115 m, the expansion deformation decreases rapidly, and the rate of decrease gradually slows down after 140 m. By drawing a reference line of 3‰ expansion deformation in the figure, it can be observed that, when the working face advances more than 65 m beyond the test point, the expansion deformation of the coal seam reaches 3‰.

The maximum expansion deformation is an important indicator for evaluating the degree of coal seam pressure relief [40]. Table 3 lists the maximum expansion deformation observed at test points P_1~P_6. The data show that, during the mining of the Wu_8 coal seam, the maximum expansion deformation of the $Ding_6$ coal seam ranges from 9.89‰ to 13.55‰. According to Article 55 of the "*Detailed Rules for Preventing Coal and Gas Outbursts*", [41] considering that all measured expansion deformations are greater than 3‰, it can be in-

ferred that the mining of the $Wu_{8\text{-}31220}$ working face has a protective effect on the overlying $Ding_{6\text{-}32070}$ working face.

Table 3. Maximum expansion deformation of $Ding_{6\text{-}32070}$ working face.

Test Point	Distance from $Wu_{8\text{-}31220}$ Starting Cut/m	Actual Maximum Expansion Deformation/‰
P_1	350	10.83
P_2	550	11.32
P_3	800	12.63
P_4	1000	13.55
P_5	1100	11.13
P_6	1200	9.89

5.3. Pressure Relief Gas Extraction Volume in the Ding$_6$ Coal Seam

The gas extraction volume of the $Ding_{6\text{-}32070}$ working face shows a certain trend over time, as shown in Figure 10. In the initial three months of gas extraction, the gas extraction volume is relatively high, which is the result of concentrated gas release in the early stage of extraction. However, over time, the gas extraction volume gradually decreases, which is due to the decrease in coal seam expansion and the slowing down of gas release.

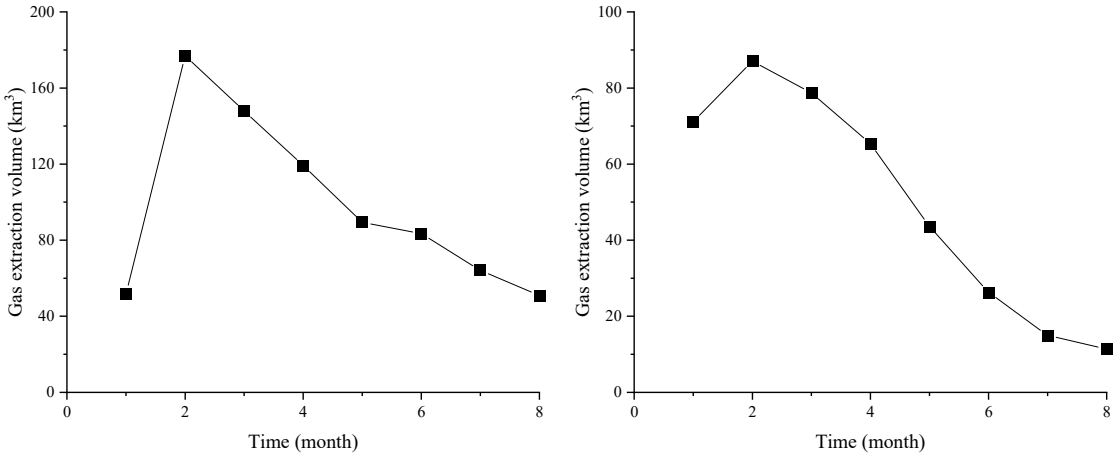

(**a**) First extraction unit (**b**) Second extraction unit

Figure 10. Gas extraction volume from the depressurized $Ding_{6\text{-}32070}$ working face.

Gas extraction data from the $Wu_{8\text{-}31220}$ mining phase demonstrate significant methane production differentials across the $Ding_{6\text{-}32070}$ drainage system, with the cumulative extraction reaching 1.18 million m^3. The intake airway's drainage network yielded 783,884 m^3 (66.4% of total) from Unit I versus 398,565 m^3 (33.6%) in Unit II. Monthly extraction volatility ranged from 50,956~176,956 m^3/month in Unit I to 11,414~87,063 m^3/month in Unit II. This indicates that there are certain differences in gas extraction volumes in different areas of the working face, which may be affected by geological structures, coal seam conditions, and other factors.

Reservoir analysis indicates 3.79 million m^3 of gas reserves in the $Ding_{6\text{-}32070}$ working face, with current pressure relief extraction achieving 31.2% recovery efficiency (1.18 million m^3). The overall gas content of the $Ding_{6\text{-}32070}$ working face is not high, and the limited number of cross-seam boreholes designed is an important reason for the low gas extraction rate. The substantial inter-seam spacing induces rapid borehole integrity degradation and constrained drainage radius. Future operations should prioritize in-seam horizontal drilling networks to enhance gas capture efficiency.

6. Conclusions

This investigation focuses on the $Wu_{8\text{-}31220}$ working face of Pingdingshan Tianan Coal Industry's No. 1 Mine and its overlying $Ding_{6\text{-}32070}$ working face, employing integrated theoretical modeling and in situ monitoring to elucidate the pressure relief mechanism of the lower protective Wu_8 coal seam and its gas synergistic control effects on the overlying $Ding_6$ seam. Key findings include the following:

(1) Gas pressure distribution analysis reveals consistent measurements (0.15–0.36 MPa) along both dip and strike directions within the pressure relief boundary and 15 m interior zone. Notably, these values represent only 23.81–57.14% of the gas pressure observed 15 m beyond the boundary, demonstrating significant pressure attenuation. This spatial pattern conclusively validates the effective pressure relief performance achieved through $Wu_{8\text{-}31220}$ mining operations, establishing optimal preconditions for subsequent gas drainage implementation.

(2) With the advance of the $Wu_{8\text{-}31220}$ working face, the overlying $Ding_6$ coal seam shows a change law of first compression and then expansion. Within the protective range demarcation boundary, the maximum expansion deformation reaches 9.89~13.55‰. Under the conditions of a borehole spacing of 20 m and extraction lasting 8 months, the pressure relief gas extraction effect of the $Ding_{6\text{-}32070}$ working face is significant, with the extraction volume accounting for 31.22% of the gas reserves, effectively reducing the gas content of the working face, lowering the risk of gas overrun, and ensuring the safe production of the mine.

(3) In the dip direction, the pressure relief angle of the Wu_8 coal seam on the intake roadway side is 77°, and the pressure relief range of the $Ding_6$ coal seam is staggered inward by 17.3 m from the intake roadway. On the return roadway side, the pressure relief angle is 83°, and the pressure relief range of the $Ding_6$ coal seam is staggered inward by 9.2 m from the return roadway. In the horizontal direction, the horizontal pressure relief angles of the Wu_8 coal seam on the starting cut and the stopping line are both 60°, and the pressure relief range of the $Ding_6$ coal seam is staggered inward by 43 m from both the starting cut and the stopping line. These precise pressure relief ranges and angle data provide an important theoretical basis for optimizing protective layer mining design and rationally arranging gas extraction boreholes. This methodology effectively resolves the spatial–temporal coordination challenges between gas extraction efficiency and operational safety in deep protective layer mining operations.

Author Contributions: Conceptualization, Y.T., Q.L. and C.Z.; methodology, Q.L. and C.Z.; software, Y.W.; validation, Y.T., Q.L., Q.W. and C.Z.; formal analysis, Y.T. and Q.L.; investigation, Y.T., Q.W. and Y.W.; resources, Y.T. and Q.W.; data curation, Q.W. and Y.W.; writing—original draft preparation, Y.T.; writing—review and editing, Q.L. and C.Z.; visualization, Y.W.; supervision, Y.T. and Q.W.; project administration, Y.T. and Q.W.; funding acquisition, Q.L. and C.Z. All authors have read and agreed to the published version of the manuscript.

Funding: This work was funded by the National Natural Science Foundation of China (52174211), Longyan City Wuping County Qimai Science and Technology Innovation Fund Project (2022LYQM007), Scientific Research Foundation of Longyan University (LB2022004).

Institutional Review Board Statement: Not applicable.

Informed Consent Statement: Not applicable.

Data Availability Statement: The data presented in this study are available on request from the corresponding author. The data are not publicly available due to privacy.

Conflicts of Interest: Authors Yanjun Tong and Qinming Wang were employed by the company Pingdingshan Tianan Coal Mining Co., Ltd. The remaining authors declare that the research was conducted in the absence of any commercial or financial relationships that could be construed as a potential conflict of interest.

References

1. Zhou, Y.; Li, H.; Huang, J.; Zhang, R.; Wang, S.; Hong, Y.; Yang, Y. Influence of coal deformation on the knudsen number of gas flow in coal seams. *Energy* **2021**, *233*, 121161. [CrossRef]
2. Guo, J.; Chen, C.; Liu, Y.; Wen, H.; Quan, Y. Response characteristics of molecular active structure of coal of different metamorphic degree to extractant. *Energy* **2025**, *320*, 135372. [CrossRef]
3. Shen, S.; Wang, H.; Ren, T.; Wang, Z. Research on the pore structure and gas adsorption/desorption characteristics of tectonic coal in minor fault zone: Implications for coal and gas outbursts. *Powder Technol.* **2025**, *456*, 120846. [CrossRef]
4. Yue, J.; Xu, J.; Zhang, J.; Shi, B.; Zhang, M.; Li, Y.; Wang, C. Gas displacement characteristics during the water wetting process of gas-bearing coal and microscopic influence mechanism. *Sci. Total Environ.* **2024**, *949*, 175034. [CrossRef]
5. Dazhao, S.; Qiang, L.; Liming, Q.; Jianguo, Z.; Khan, M.; Yujie, P.; Yingjie, Z.; Man, W.; Minggong, G.; Taotao, H. Experimental study on resistivity evolution law and precursory signals in the damage process of gas-bearing coal. *Fuel* **2024**, *362*, 130798. [CrossRef]
6. Jin, Y.; Tong, X.; Zheng, X.; Li, Y.; Dong, B. Risk assessment of coal and gas outbursts driven by the theory of three types of hazards coupled with 80 accident cases. *Saf. Sci.* **2025**, *184*, 106771. [CrossRef]
7. Qiu, L.; Dang, J.; Zhang, J.; Wang, M.; Liu, Q.; Si, L.; Jiang, Z.; Khan, M. Investigating nonlinear resistivity characteristics and mechanisms of coal during various loading stages. *J. Appl. Geophys.* **2025**, *238*, 105705. [CrossRef]
8. Anani, A.; Adewuyi, S.O.; Risso, N.; Nyaaba, W. Advancements in machine learning techniques for coal and gas outburst prediction in underground mines. *Int. J. Coal Geol.* **2024**, *285*, 104471. [CrossRef]
9. Li, M.; Lu, S.; Wei, C.; Li, Z.; Ye, Q.; Zhang, Y. Study on energy instability mechanism of composite coal seam based on the coupling effect of damage and unsteady diffusion. *Fuel* **2025**, *379*, 133051. [CrossRef]
10. Wang, C.; Liu, L.; Li, X.; Xu, C.; Li, K. Mechanism of gas pressure action during the initial failure of coal containing gas and its application for an outburst inoculation. *Int. J. Min. Sci. Technol.* **2023**, *33*, 1511–1525. [CrossRef]
11. Yang, G.; Song, D.; Wang, M.; Qiu, L.; He, X.; Khan, M.; Qian, S. New insights into dynamic disaster monitoring through asynchronous deformation induced coal-gas outburst mechanism of tectonic and raw coal seams. *Energy* **2024**, *295*, 131063. [CrossRef]
12. Li, W.; Jia, T.; Zhu, Y.; Guo, S. Study on the influence of stress distribution in fault structural zones on coal and gas outbursts. *Min. Metall. Explor.* **2025**, *42*, 719–735. [CrossRef]
13. Zhao, Y.; Song, D.; Qiu, L.; Khan, M.; He, X.; Li, Z.; Peng, Y.; Wang, A. An efficient coal and gas outburst hazard prediction method using an improved limit equilibrium model and stress field detection. *Int. J. Coal Sci. Technol.* **2025**, *12*, 23. [CrossRef]
14. Vassilyev, I.; Mendakulov, Z.; Imansakipova, B.; Aitkazinova, S.; Issabayev, K.; Imansakipova, N.; Madimarova, G. Acoustic emission spectrum for mine hazards identification and prevention. *Sci. Rep.* **2025**, *15*, 6408. [CrossRef] [PubMed]
15. Zhang, C.; Wang, P.; Wang, E.; Chen, D.; Li, C. Characteristics of coal resources in china and statistical analysis and preventive measures for coal mine accidents. *Int. J. Coal Sci. Technol.* **2023**, *10*, 22. [CrossRef] [PubMed]
16. Wang, X.; Tian, C.; Wang, Q.; Shi, Z.; Sun, Y.; Wang, K. Study on influencing factors and prevention measures of coal-rock-gas compound dynamic disaster in deep coal mine mining. *Sci. Rep.* **2025**, *15*, 2080. [CrossRef]
17. Yang, W.; Wang, W.; Jia, R.; Walton, G.; Sinha, S.; Chen, Q.; Lin, B.; Jiao, X. Parameter optimization of coal face blasting for coal and gas outburst control. *Bull. Eng. Geol. Environ.* **2023**, *82*, 80. [CrossRef]
18. Zhang, G.; Wang, E. Risk identification for coal and gas outburst in underground coal mines: A critical review and future directions. *Gas Sci. Eng.* **2023**, *118*, 205106. [CrossRef]
19. Zhou, A.; He, Y.; Wang, K.; Li, B.; Wang, Y.; Yang, Y. Hydraulic fracture propagation in soft coal composite reservoirs: Mechanical responses and energy dissipation mechanisms. *Int. J. Min. Sci. Technol.* **2025**, *35*, 573–588. [CrossRef]
20. Cheng, X.; Zhao, G.; Li, Y.; Meng, X.; Tu, Q. Key technologies and engineering practices for soft-rock protective seam mining. *Int. J. Min. Sci. Technol.* **2020**, *30*, 889–899. [CrossRef]
21. Lei, W.; Du, X.; Zhang, D.; Wang, J.; Yang, R.; Zheng, C.; Huang, X.; Wang, S.; Zhao, J.; Cao, J. Sensitivity analysis of geological mining influencing factors on the pressure relief effect of upper protective layer mining. *Energy Sci. Eng.* **2024**, *12*, 4703–4719. [CrossRef]
22. Yang, W.; Zhang, W.; Lin, B.; Si, G.; Zhang, J.; Wang, J. Integration of protective mining and underground backfilling for coal and gas outburst control: A case study. *Process Saf. Environ.* **2022**, *157*, 273–283. [CrossRef]
23. Lu, A.; Song, D.; Li, Z.; He, X.; Dou, L.; Xue, Y.; Yang, H. Numerical simulation study on pressure-relief effect of protective layer mining in coal seams prone to rockburst hazard. *Rock. Mech. Rock. Eng.* **2024**, *57*, 6421–6440. [CrossRef]

24. Zhang, H.; Wen, Z.; Yao, B.; Chen, X. Numerical simulation on stress evolution and deformation of overlying coal seam in lower protective layer mining. *Alex. Eng. J.* **2020**, *59*, 3623–3633. [CrossRef]
25. Xie, H.; Li, X.; Cai, J.; Wang, S.; Feng, C. Evolution of fissures and pressure discharge of gas caused by mining of the upper protective layer of a coal seam. *Sci. Rep.* **2023**, *13*, 2561. [CrossRef]
26. Yang, W.; Lin, B.; Qu, Y.; Zhao, S.; Zhai, C.; Jia, L.; Zhao, W. Mechanism of strata deformation under protective seam and its application for relieved methane control. *Int. J. Coal Geol.* **2011**, *85*, 300–306. [CrossRef]
27. Wang, H.; Wang, E.; Li, Z.; Shen, R.; Liu, X.; Zhang, Q.; Li, B. Study and application of dynamic inversion model of coal seam gas pressure with drilling. *Fuel* **2020**, *280*, 118653. [CrossRef]
28. Liu, C.; Man, Z.Y.; Li, M.L. Study on the dynamic evolution of mining-induced stress and displacement in the floor coal-rock induced by protective layer mining. *Minerals* **2024**, *14*, 1084. [CrossRef]
29. Cheng, Z.; Pan, H.; Zou, Q.; Li, Z.; Chen, L.; Cao, J.; Zhang, K.; Cui, Y. Gas flow characteristics and optimization of gas drainage borehole layout in protective coal seam mining: A case study from the shaqu coal mine, Shanxi province, China. *Nat. Resour. Res.* **2021**, *30*, 1481–1493. [CrossRef]
30. Li, L.; Wu, G.Y.; Liu, Q.Z. Study on overburden movement and fissure evolution law of protective layer mining in shallow coal seam. *Energies* **2022**, *15*, 1831. [CrossRef]
31. Jin, K.; Cheng, Y.; Wang, W.; Liu, H.; Liu, Z.; Zhang, H. Evaluation of the remote lower protective seam mining for coal mine gas control: A typical case study from the zhuxianzhuang coal mine, huaibei coalfield, china. *J. Nat. Gas Sci. Eng.* **2016**, *33*, 44–55. [CrossRef]
32. Wang, L.; Lu, Z.; Chen, D.; Liu, Q.; Chu, P.; Shu, L.; Ullah, B.; Wen, Z. Safe strategy for coal and gas outburst prevention in deep-and-thick coal seams using a soft rock protective layer mining. *Saf. Sci.* **2020**, *129*, 104800. [CrossRef]
33. Li, Y.; Yu, K.; Wan, Z.; Zhang, Y.; Wang, Z.; Shi, P.; Zhen, Z.; Zhang, B. Regional structural controls on a hydrothermal geothermal system in the eastern pingdingshan coalfield, China: A comprehensive review. *Geothermics* **2024**, *123*, 103131. [CrossRef]
34. Ullah, B.; Cheng, Y.; Wang, L.; Hu, B.; Jiskani, I.M.; Hassan, F.U.; Shahani, N.M.; Ali, M. Experimental and theoretical analyses to predict coal and gas outburst using desorption indices of drill cuttings. *Arab. J. Geosci.* **2022**, *15*, 665. [CrossRef]
35. Chai, Y.J.; Dou, L.M.; He, J.; Ma, X.T.; Lu, F.Z.; He, H. Limitations of upper protective layers as pressure relief measures for extra-thick coal seam mining: Insights from a case study. *Energies* **2024**, *17*, 1446. [CrossRef]
36. Shang, Y.Q.; Wang, Y.; Zhang, L.; Wu, G.Y.; Kong, D.Z.; Zhang, P.F.; Jia, T.P. Impact of lower protective coal seam mining on overlying strata: Deformation, pressure relief, and permeability enhancement. *Int. J. Geomech* **2024**, *24*, 04024178. [CrossRef]
37. Xiao, J.; Chen, X.X.; Li, S.G.; Bi, R.Q.; Chen, Z.H. Analyzing the optimization of unloading gas extraction drilling arrangement based on stress distribution in the protected layer. *Sustainability* **2024**, *16*, 2133. [CrossRef]
38. Peng, N.B.; Zhang, C.L.; Feng, R.M.; Arif, A.; Chen, X.; Zhang, W.D.; Zhang, S.; Feng, M.J. Analysis of dynamic evolution of surrounding rock movement and stress-fracture in the upward and repeated mining of close-distance coal seams. *Adv. Civ. Eng.* **2024**, *2024*, 5548837. [CrossRef]
39. Shi, Z.S.; Zhao, H.W.; Qin, B.; Liang, B.; Hao, J.F. Experimental study on rock strata movement and stope stress distribution law under mining height regulation. *Energy Sci. Eng.* **2024**, *12*, 1531–1550. [CrossRef]
40. Ma, J.H.; Hou, C.; Hou, J.T. Numerical and similarity simulation study on the protection effect of composite protective layer mining with gently inclined thick coal seam. *Shock Vib.* **2021**. [CrossRef]
41. National Coal Mine Safety Administration. *Detailed Rules for Preventing Coal and Gas Outbursts*; China Coal Industry Publishing House: Beijing, China, 2019. Available online: https://www.gov.cn/xinwen/2019-08/21/content_5423024.htm (accessed on 15 July 2024).

Disclaimer/Publisher's Note: The statements, opinions and data contained in all publications are solely those of the individual author(s) and contributor(s) and not of MDPI and/or the editor(s). MDPI and/or the editor(s) disclaim responsibility for any injury to people or property resulting from any ideas, methods, instructions or products referred to in the content.